Emergent magneto-inductance effect in permalloy thin films on flexible polycarbonate substrates at room temperature FREE

Yu Matsushima ; Zijing Zhang ; Yuri Ohashi; Tsunagu Hatakeyama ; Gang Xiao ; Takumi Funato ; Mamoru Matsuo ; Hideo Kaiju ✉

Check for updates

CHORUS

View Online

Export Citation

CrossMark

Emergent magneto-inductance effect in permalloy thin films on flexible polycarbonate substrates at room temperature

Yu Matsushima,[1] (iD) Zijing Zhang,[1] (iD) Yuri Ohashi,[1] Tsunagu Hatakeyama,[1] (iD) Gang Xiao,[2] (iD) Takumi Funato,[3,4] (iD)
Mamoru Matsuo,[4,5,6,7] (iD) and Hideo Kaiju[1,3,a)] (iD)

AFFILIATIONS

[1]Faculty of Science and Technology, Keio University, Yokohama, Kanagawa 223-8522, Japan
[2]Department of Physics, Brown University, Providence, Rhode Island 02912, USA
[3]Center for Spintronics Research Network, Keio University, Yokohama, Kanagawa 223-8522, Japan
[4]Kavli Institute for Theoretical Sciences, University of Chinese Academy of Sciences, Beijing 100190, China
[5]CAS Center for Excellence in Topological Quantum Computation, University of Chinese Academy of Sciences, Beijing 100190, China
[6]Advanced Science Research Center, Japan Atomic Energy Agency, Tokai 319-1195, Japan
[7]RIKEN Center for Emergent Matter Science, Wako, Saitama 351-0198, Japan

[a)]Author to whom correspondence should be addressed: kaiju@appi.keio.ac.jp

ABSTRACT

Emergent inductance has attracted significant interest for its relevance in both interesting fundamental physics and practical applications in magnetic devices that demand miniaturization without compromising inductance. In this Letter, we report the discovery of a stepwise magnetic field-induced emergent magneto-inductance (EML) effect in Permalloy (Py) thin films deposited on polycarbonate (PC) substrates. Remarkably, Py/PC devices exhibit an exceptionally large inductance variation exceeding 1 μH at room temperature, and intriguingly, a sign reversal of inductance occurs around the zero magnetic field. The dependencies of the EML effect on frequency, step magnetic field changes, and film width can be explained from the theory based on the spin motive force driven by transient domain wall motion. This study opens up exciting avenues for advancing our understanding of emergent inductance in fundamental physics and paves the way for practical applications in flexible magnetic devices.

Published under an exclusive license by AIP Publishing. https://doi.org/10.1063/5.0181272

In recent years, the concept of emergent inductors has garnered significant attention due to its intriguing implications for both fundamental physics and practical applications.[1–6] Emergent inductors exploit the spin motive force (SMF) generated through the current-induced motion of non-collinear spin textures.[7–11] The spin motive force V_{SMF} is given by the expression $V_{SMF} = \int di(P\hbar/2e)\mathbf{n} \cdot (\partial \mathbf{n}/\partial i \times \partial \mathbf{n}/\partial t)$, where P denotes the spin polarization, $\hbar$ is the Dirac constant, e is the elementary electric charge, $\mathbf{n}$ is a classical unit vector to represent the spin direction, i is the coordinate in the spin propagation direction, and t is the time. Recent research has highlighted that emergent inductance can arise from the collective interactions between the conduction electrons and the helical-spin textures. For instance, $Gd_3Ru_4Al_{12}$, a center-symmetric helical magnetic film, exhibits a substantial emergent inductance of $\sim$400 nH at low temperatures (around 15 K).[2] This helical magnet can assume various non-collinear spin

structures, including proper-screw, magnetic skyrmion, and transverse conical configurations, owing to the competition among the Ruderman–Kittel–Kasuya–Yosida (RKKY) interaction, magnetic anisotropy, and thermal fluctuations.[12–16]

Interestingly, the emergent inductance in $Gd_3Ru_4Al_{12}$ shows an inverse size scaling law, increasing as the element cross section decreases,[2] which contrasts with classical inductance behavior. This characteristic offers a promising solution to the size constraints associated with coil-shaped inductors based on classical electromagnetism. Moreover, the observation of emergent inductance beyond room temperature in materials like YMn_6Sn_6 (Ref. 5) or $Y_xTb_{1-x}Mn_6Sn_6$ (Ref. 6) has been reported, with inductance reaching a few μH, comparable to that of commercial inductors. Notably, in this system, the sign of inductance can be controlled, representing a previously unexplored phenomenon. Theoretical explanations for this sign reversal have been

proposed, linking it to nonadiabaticity, extrinsic pinning effects,[3] or a microscopic model involving a spiral magnet composed of one-dimensional electrons coupled with localized spins through exchange interactions.[4] The emergent inductance is associated with the tilting mode and/or phason mode, stemming from the spin dynamics of helical structures. Excitation of the spin helix by an ac current can trigger the tilting mode, leading to the out-of-plane rotation of spiral spins, and/or the phason mode, characterized by the uniform in-plane rotation of helical spins. The inductance's sign is determined by these modes. Specifically, a positive inductance sign is observed when phason excitation arises from the gapless Nambu–Goldstone mode in the absence of impurity pinning. However, with impurity pinning, the inductance sign may be positive or negative, depending on whether the frequency measured is above or below the extrinsic pinning frequency. The tilting mode typically contributes to a positive inductance. Experimentally, factors such as magnetic field, temperature, and the strength of the induced current can be manipulated to control the inductance's sign.[4–6]

Currently, the theory of emergent inductance has been extended to encompass arbitrary magnetic textures by incorporating spin–orbit (SO) couplings, particularly in the absence of spatial inversion symmetry, such as in the case of spatially uniform magnetization.[17] The emergence of SO-induced inductance arises from a dynamical Aharonov–Casher phase of an electron in the presence of both magnetism and the SO couplings. Consequently, emergent inductance of quantum mechanical origin has been predicted and experimentally demonstrated in helical-spin magnets or magnetic materials with strong SO coupling.

In this Letter, we report the observation of an emergent magneto-inductance (EML) effect, wherein both the magnitude and sign of the emergent inductance exhibit tunability in response to magnetic fields, in Permalloy (Py) thin films thermally evaporated onto polycarbonate (PC) substrates. Our methodology for inducing the EML effect in versatile ferromagnetic materials relies on the manipulation of magnetic domain walls in transient states using a stepwise magnetic field. This approach allows us to generate complex domain wall motion without the need for specialized spin texture, such as helical-spin magnets.

As a result of our experiment, we have observed a large EML effect that exceeds 1 μH, accompanied by a sign reversal of inductance within a small magnetic field of about 20 Oe, all at room temperature. Furthermore, we have characterized the frequency dependence of the emergent inductance, which follows a Debye-type relaxation profile. Notably, we have observed that the emergent inductance exhibits an inverse relationship with the thin-film width, with inductance increasing as the cross-sectional area of the films decreases. The observed EML effect can be theoretically explained by considering the SMF driven by transient domain wall motion.

Our findings not only advance our understanding of unconventional inductance but also offer promising prospects for practical applications in the realm of flexible magnetic electronics. These applications include but not limited to wearable electronics, compact compasses, highly sensitive sensors, and motion detectors.[18–21]

The Py thin films were thermally evaporated onto PC substrates (1.0–2.5 mm in width, 15.0 mm in length, and 40.3 μm in thickness) in a high vacuum chamber with a base pressure of ~10^{-6} Pa. The choice PC[22] as a substrate was motivated by its exceptional planarity, rendering it an ideal flexible substrate for supporting magnetic metallic thin films, as compared to alternative materials such as polyvinylidene fluoride (PVDF)[23] or polyethylene naphthalate (PEN).[24,25] During the deposition process, the PC substrates were subjected to a magnetic field of 360 Oe oriented in parallel to the surface and aligned along the short axis [x axis in Fig. 1(a)] of the PC substrate. This magnetic field configuration was employed to induce a transverse magnetic anisotropy in the Py layers. The growth rate of Py thin films was maintained
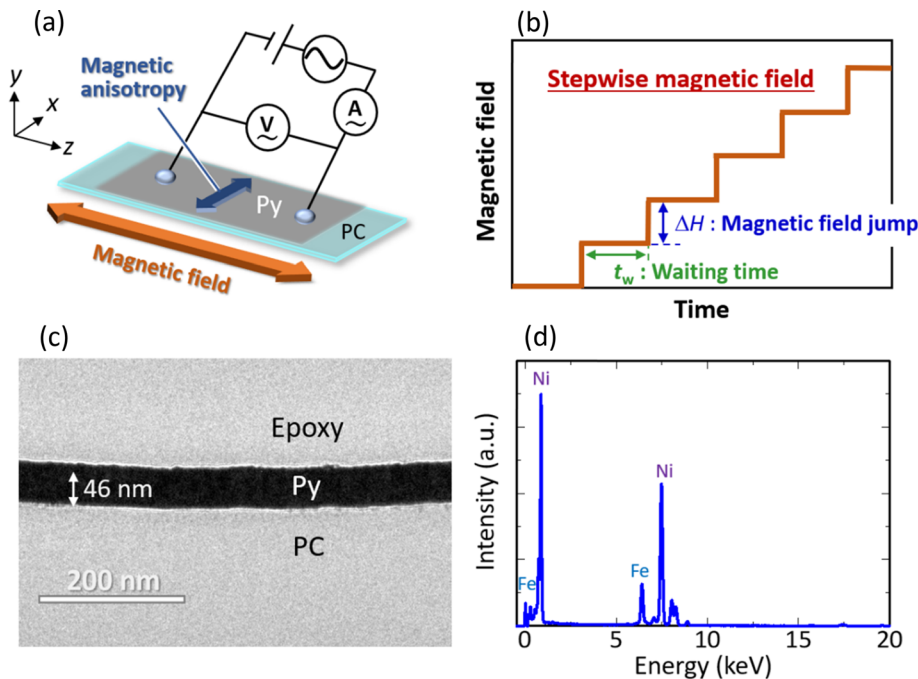
FIG. 1. (a) Schematic of the Py/PC sample structure and the measurement setup of emergent inductance, (b) stepwise magnetic field profile (characterized by jump ΔH and waiting time) used in our measurements, (c) cross-sectional TEM image of Py (46 nm)/PC, and (d) TEM-EDS spectrum of Py.

at 1–2 nm/min at an evaporation power of 200 W. The microstructures and the interfacial characteristics of the Py/PC interface were examined by using a transmission electron microscope (TEM, Thermo Fisher Scientific, TECNAI Osiris) operating at 200 kV. The energy dispersive spectroscopy (EDS) was used to determine elemental composition of Py. The cross-sectional TEM–EDS samples were prepared using a combination of microtome slicing and mechanical polishing. The magnetic properties were measured by using a focused magneto-optical Kerr effect (MOKE) magnetometer (NEOARK, BH-PI920-HU) under a magnetic field of up to 1 kOe at room temperature. To assess the frequency responses of emergent inductance in Py/PC, we employed an AC two-probe method using an LCR meter (KEYSIGHT TECHNOLOGIES, 4284A) at room temperature, as shown in Fig. 1(a). The distance between two probes is 10 mm. The AC voltage was set at 100 mV$_{rms}$, and the frequency range spanned from 4 to 48 kHz. The DC voltage was less than 1 mV. Magnetic fields were applied along the longitudinal direction (z axis) of the films up to 200 Oe. A *stepwise* magnetic field sweep, as depicted in Fig. 1(b), was employed to induce non-collinear spin textures.

Figure 1(c) shows the cross-sectional TEM image of Py/PC, encapsulated with a protective epoxy layer, revealing distinct and indicating sharp and flat interfaces between Py and PC. Additionally, Fig. 1(d) presents the TEM-EDS spectrum of Py, from which the atomic composition of the film was determined. The atomic composition of the Ni and Fe elements was evaluated to be 79% and 21%, respectively.

Figures 2(a)–2(c) show the magnetic field transfer curves of the emergent inductance in Py/PC with a film width w of 2.5 mm at frequencies of 4, 12, and 48 kHz. The magnetic field jump (ΔH) is 2 Oe, and the waiting time t_w of the stepwise field is 0.1 s. The emergent inductance L_{SMF} is quantitatively expressed by the following equation:

$$L_{SMF} = [(X - X_s)/\omega], \qquad (1)$$

where X is the measured reactance of the devices, X_s is the reference reactance obtained under a sufficiently large magnetic field of 200 Oe, where the magnetization reaches saturation, and ω is the angular frequency. The equivalent circuit, shown in Fig. S1(a), is used for the measurement of L_{SMF} from X and X_s in Eq. (1). The detailed measurement method is described in the supplementary material [see Figs. S1(b)–S1(d) and S2]. As shown in Figs. 2(a)–2(c), the emergent inductance L_{SMF} undergoes significant changes within the vicinity of the zero-field region, accompanied by alterations in its sign. At 4 kHz, the maximum (minimum) emergent inductances, $L_{max(min)}$, are recorded as 197 nH and −228 nH. Here, we define the inductance change as $\Delta L = L_{max} - L_{min}$. The observed inductance changes ΔL amount to 425 nH at 4 kHz, 127 nH at 12 kHz, and 13 nH at 48 kHz. The EML curves at different frequencies are detailed in Fig. S3. Furthermore, Fig. 2(d) demonstrates that the emergent inductance exhibits an upward trend as the frequency decreases.

The purpose of implementing the stepwise magnetic field sweep, as illustrated in Fig. 1(b), is to control probability of domain wall injection. In Figs. 3(a)–3(c), we explore the effect of the field jump (ΔH) on the EML effect while maintaining a waiting time of 0.1 s. It is evident that a larger ΔH intensifies the EML effect, whereas a prolonged waiting time diminishes it, as shown in Figs. S1(c) and S2. This observation strongly indicates that the EML effect is caused by the transient domain walls induced by the stepwise magnetic field. The inductance change (ΔL) associated with the EML effect exhibits an escalation from 217 to 766 nH with increasing ΔH values from 1 to 4 Oe. Notably, Fig. 3(d) illustrates that the EML effect scales approximately with ΔH. Further insights into the ΔH dependence of the EML curves at 12 and 24 kHz can be found in Fig. S4.
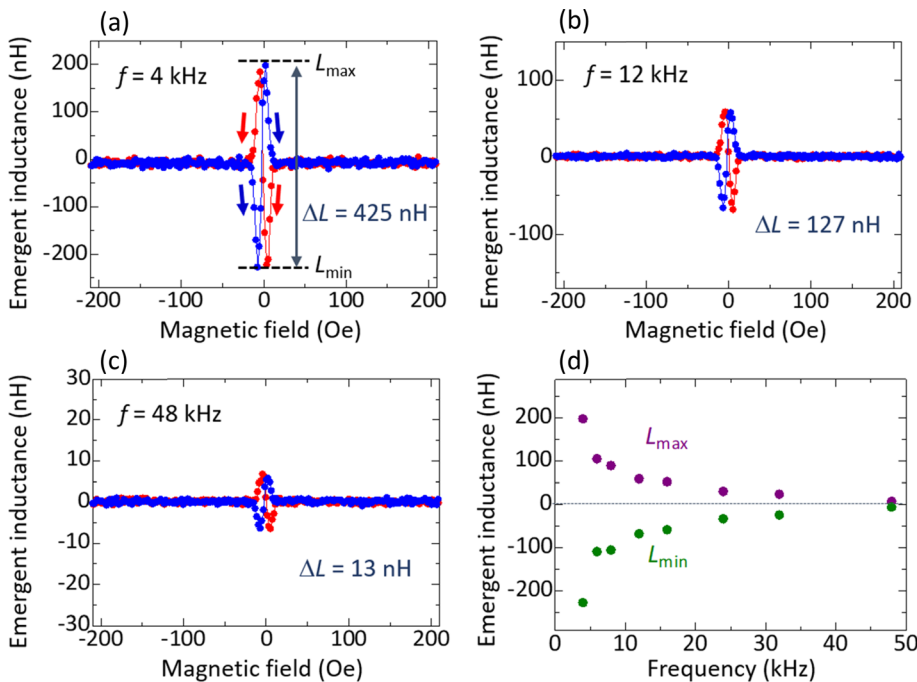
FIG. 2. EML curves of Py/PC under a magnetic field variation ΔH of 2 Oe and a waiting time of 0.1 s at (a) 4, (b) 12, and (c) 48 kHz. The blue (red) plots represent the results obtained under the forward (reverse) sweeping field. (d) Plots of maximum (minimum) emergent inductance $L_{max(min)}$ in the frequency range of 4–48 kHz.
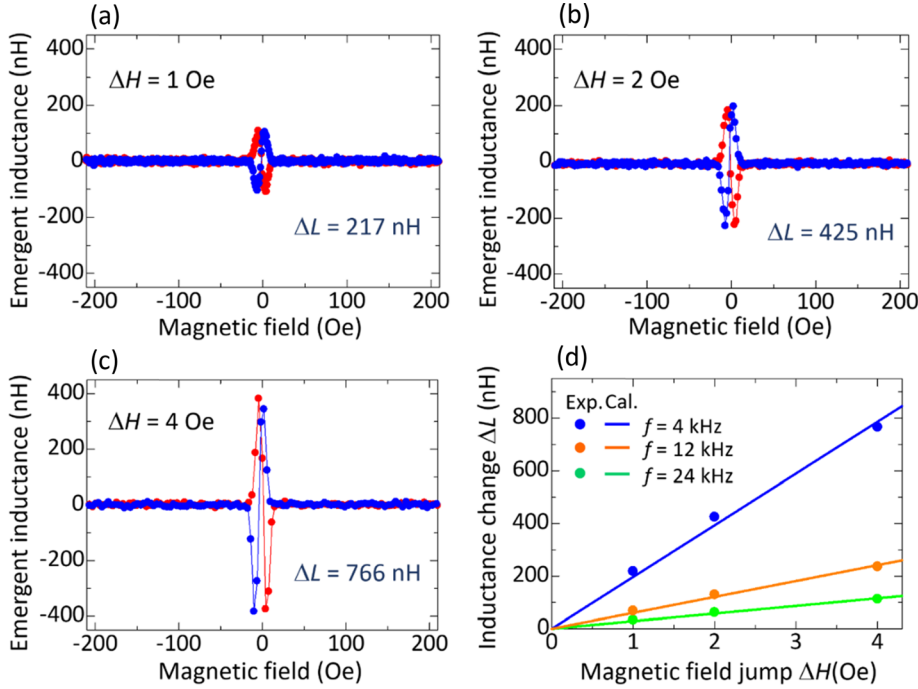
FIG. 3. EML curves in Py/PC with a film width w of 2.5 mm at 4 kHz with a magnetic field jump ΔH of (a) 1, (b) 2, and (c) 4 Oe. The waiting time t_w is set at 0.1 s. (d) ΔH dependence of inductance change ΔL in the EML effect.

In this section, we delve into the underlying mechanism behind the observed EML effect, which can be explained from the SMF driven by domain wall motion. The overall emergent inductance $L_{\text{SMF}}^{\pm}$ can be expressed as follows:

$$L_{\text{SMF}}^{\pm} = \pm N_{\text{dw}}\tanh(H/H_s)L_{\text{dw}}, \quad (2)$$

where the upper (lower) sign of $L_{\text{SMF}}^{\pm}$ corresponds to the forward (reverse) sweeping direction of magnetic field. The sign change ($+$ or $-$) indicates the reversal of the emergent inductance in response to the time-varying magnetic field, either increasing or decreasing; $\partial H/\partial t > 0$ or $\partial H/\partial t < 0$. N_{dw} is the number of domain walls, L_{dw} is the emergent inductance originating from one domain wall motion, and H_s is the saturation magnetic field. Since domain wall structures are potentially determined by the contribution of magnetic anisotropy, thermal fluctuations, and Zeeman energy, the domain wall orientation can be typically expressed by the tangent hyperbolic function such as $\tanh(H/H_s)$. Here, the number of domain walls N_{dw} in the films can be estimated from Figs. 3, S1(c), and S2. Based on the results shown in Fig. 3, it is plausible to posit that the magnetic field jump ΔH determines the quantity of domain walls present. From Figs. S1(c) and S2, it is suggested that the domain walls vanish when the waiting time for the stepwise magnetic field t_w exceeds a certain threshold time, reaching the steady state t_0. Assuming the thermal excitation follows a Boltzmann distribution based on Zeeman energy, the number of domain walls is given by

$$N_{\text{dw}} = \alpha_1 \Delta H \exp\left(-\alpha_2 \frac{\boldsymbol{M} \cdot \boldsymbol{H}}{k_B T}\right)\Theta(t_0 - t_w), \quad (3)$$

where $\boldsymbol{M}$ is the magnetization vector of ferromagnetic thin films, $\boldsymbol{H}$ is the external magnetic field vector, k_B is the Boltzmann constant, T is the temperature, $\Theta(t)$ is the Heaviside step function, and α_1 and α_2 are the fitting

parameters. To derive the emergent inductance L_{dw}, we focus on the motion of a single domain wall, described by the collective coordinates that include center-of-mass position X_{dw} and polarization angle out of the easy plane ϕ_{dw} as shown in Fig. 4(a). We introduce a classical unit vector to represent the spin direction $\boldsymbol{n} = (\sin\theta_{\text{dw}}\cos\phi_{\text{dw}}, \sin\theta_{\text{dw}}\sin\phi_{\text{dw}}, \cos\theta_{\text{dw}})$. This way, X_{dw} is specialized by $\cos\theta_{\text{dw}} = \tanh[(z - X_{\text{dw}})/\lambda_{\text{dw}}]$. The equation governing the motion of domain wall in response to the AC density j_{ac} is given by[1,26–28]

$$\frac{\dot{X}_{\text{dw}}}{\lambda_{\text{dw}}} - \alpha_G\dot{\phi}_{\text{dw}} = \frac{v_c}{2\lambda_{\text{dw}}}\sin 2\phi_{\text{dw}} + \frac{a^3 P}{2eS\lambda_{\text{dw}}}j_{\text{ac}}, \quad (4)$$

$$\dot{\phi}_{\text{dw}} + \alpha_G\frac{\dot{X}_{\text{dw}}}{\lambda_{\text{dw}}} = f_{\text{pin}} + \beta\frac{a^3 P}{2eS\lambda_{\text{dw}}}j_{\text{ac}}, \quad (5)$$

where λ_{dw} is the domain wall width, α_G is the Gilbert damping constant, S is the spin quantum number, a is the lattice constant, and β represents the non-adiabatic coefficient. Note that the dc external magnetic field can be neglected due to no contribution to the emergent inductance. Here, the intrinsic pinning coming from the hard-axis magnetic anisotropy $K_\perp$ can be expressed as the unit of velocity $v_c = K_\perp\lambda_{\text{dw}}S/\hbar$. f_{pin} is given by $f_{\text{pin}} = -(\lambda_{\text{dw}}/\hbar n_s S)F_{\text{pin}}$, where n_s is the number of localized spins in the domain wall. $F_{\text{pin}} = -\partial V_{\text{pin}}/\partial X_{\text{dw}}$ is the force due to the pinning potential V_{pin},

$$V_{\text{pin}}(X_{\text{dw}}) = N_s V_0\left[(X_{\text{dw}}/\xi)^2 - 1\right]\Theta(\xi - |X_{\text{dw}}|), \quad (6)$$

where N_s is the number of spins in the domain wall, V_0 is the magnitude of the pinning potential, and pinning range ξ is of order of domain wall width λ_{dw} in most cases. Therefore, we derive

$$f_{\text{pin}} = -v_{\text{pin}}\frac{X_{\text{dw}}}{\lambda_{\text{dw}}^2}\Theta(\xi - |X_{\text{dw}}|), \quad (7)$$
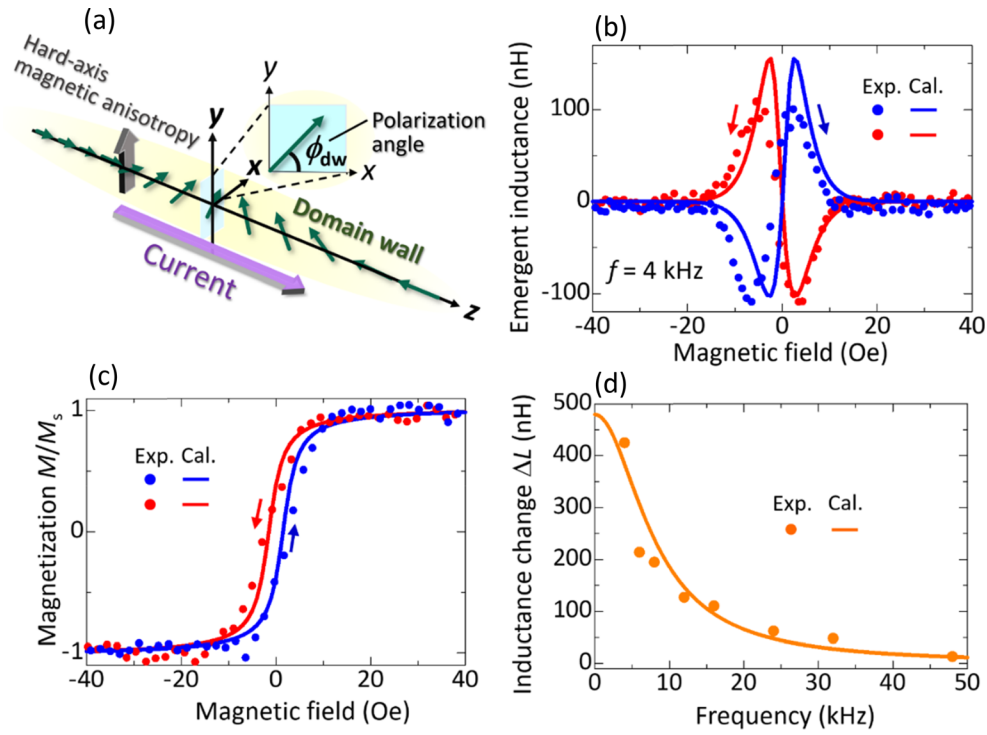
FIG. 4. (a) Schematic of current-driven domain wall motion in the films. (b) Experimental and calculation results of EML curves at 4 kHz in Py/PC with a film width of 2.5 mm and $\Delta H = 1$ Oe. (c) Magnetization curves of Py thin films on PC substrates. (d) Frequency characteristics of inductance change ΔL in the EML effect.

where the impurity pinning potential can be expressed as the unit of velocity $v_{\mathrm{pin}} = 2V_0\lambda_{\mathrm{dw}}^3/\hbar S\xi^2$. Here, we assume that the domain wall motion occurs within the range of the pinning potential. Considering the linear response of the ac current j_{ac} and performing Fourier transformation, the polarization angle ϕ_{dw} is determined by

$$\phi_{\mathrm{dw}}(\omega) = \frac{\zeta j_{\mathrm{ac}}(\omega)}{\lambda_{\mathrm{dw}}}$$
$$\cdot \frac{i\omega(\beta - \alpha_{\mathrm{G}}) + v_{\mathrm{pin}}/\lambda_{\mathrm{dw}}}{\left(1 + \alpha_{\mathrm{G}}^2\right)\omega^2 + i\alpha_{\mathrm{G}}\omega(v_{\mathrm{c}} + v_{\mathrm{pin}})/\lambda_{\mathrm{dw}} - v_{\mathrm{c}}v_{\mathrm{pin}}/\lambda_{\mathrm{dw}}^2}, \quad (8)$$

where $\zeta = a^3 P/2eS$. Under the assumption of $\alpha_{\mathrm{G}} \sim \beta \ll 1$, $v_{\mathrm{pin}} \ll v_{\mathrm{c}}$, and $v_{\mathrm{c}}v_{\mathrm{pin}}/\lambda_{\mathrm{dw}}^2 \gg \omega^2$, the polarization angle reduces to the following Debye-type relaxation form:

$$\phi_{\mathrm{dw}}(\omega) = \frac{\zeta j_{\mathrm{ac}}(\omega)}{v_{\mathrm{c}}} \cdot \frac{1}{i\omega\tau - 1}, \quad (9)$$

where $\tau = \alpha_{\mathrm{G}}\lambda_{\mathrm{dw}}/v_{\mathrm{pin}}$ is the relaxation time of the polarization angle. The validity of the assumption is described in the supplementary material. Thus, the emergent inductance L_{dw} is obtained as

$$L_{\mathrm{dw}}(\omega) = \mathrm{Re}\left[-\frac{P\pi\hbar\phi_{\mathrm{dw}}(\omega)}{2eAj_{\mathrm{ac}}(\omega)}\right] = \mathrm{Re}\left[\frac{P\pi\hbar\zeta}{2ev_{\mathrm{c}}A} \cdot \frac{1}{1 - i\omega\tau}\right], \quad (10)$$

where A is the cross section area of the sample in the x–y plane. Substituting Eqs. (3) and (10) into Eq. (2) yields the inductance in the EML effect. Figure 4(b) shows the calculation and experimental results of EML curves at 4 kHz. To estimate the Zeeman energy, $-\boldsymbol{M} \cdot \boldsymbol{H}$, in

Eq. (3), we use the normalized magnetization M/M_{s} obtained from the MOKE shown in Fig. 4(c). The MOKE signal reveals that the coercive force is about 2 Oe, indicating that the fabricated Py thin films are magnetically soft. To compensate for a small number of MOKE measurement points, we introduce an approximate curve using the arctan function for the calculation of the magnetization. The detailed arctan function including the parameters is shown in the supplementary material, Table S1. As shown in Fig. 4(b), the calculation results of EML curves are in good agreement with the experimental data. The fitting parameters are described in Table S2. The modeling results of EML curves at different frequencies are shown in Fig. S5, and the parameters are demonstrated in Table S2. Furthermore, from Eqs. (2), (3), and (10), the inductance change ΔL can be expressed by

$$\Delta L(\omega) = L_{\max} - L_{\min}$$
$$= \frac{|\Upsilon(H = H_{\max})| + |\Upsilon(H = H_{\min})|}{A} \cdot \mathrm{Re}\left[\frac{1}{1 - i\omega\tau}\right], \quad (11)$$

where $H_{\max(\min)}$ is the magnetic field, at which the inductance shows the maximum (minimum) value of $L_{\max(\min)}$, and we define $\Upsilon = [N_{\mathrm{dw}}(H, \Delta H)P\pi\hbar\zeta\tanh(H/H_{\mathrm{s}})]/2ev_{\mathrm{c}}$. The calculation using Eq. (11) provides the quantitative understanding of the frequency-dependent characteristics. Here, according to the results shown in Fig. 2(d), we can construct the frequency profile of the inductance change ΔL based on the observed EML curves. As shown in Fig. 4(d), the calculation results fit to experimental data well. The fitting parameters used in the calculation are described in Table S3. This result indicates that the frequency dependence of EML can be comprehensively
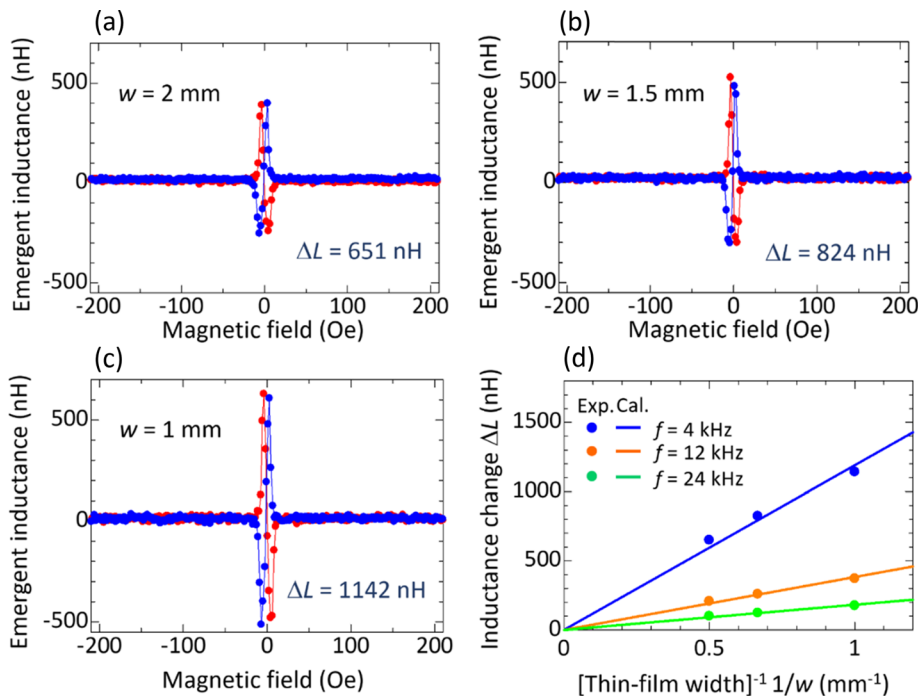
FIG. 5. EML curves of Py/PC with a thin-film width of (a) 2, (b) 1.5, and (c) 1 mm at 4 kHz under a magnetic field variation ΔH of 2 Oe. (d) Thin-film width dependence of inductance change ΔL in the EML effect.

explained through a Debye-type relaxation mechanism, primarily driven by extrinsic pinning. The Debye-type modeling is consistent with the frequency response of emergent inductance observed in materials such as $Gd_3Ru_4Al_{12}$ (Ref. 2) and YMn_6Sn_6 (Ref. 5). The dependence of the emergent inductance L_{SMF} on the ac electric field E_{ac} is a significant aspect to consider. According to the theory based on Eqs. (2), (3), and (9), L_{SMF} is independent of E_{ac}. The detailed theory and the corresponding measurement results are elaborated in the supplementary material. In addition, Eq. (11) highlights the inverse proportionality between the emergent inductance and the film width. As shown in Figs. 5(a)–5(c), the inductance change ΔL exhibits an upward trend with decreasing film width. Particularly noteworthy is the observation of an exceptionally large inductance change ΔL, amounting to 1143 nH at $f = 4$ kHz, $\Delta H = 2$ Oe, and $w = 1$ mm. It is noted that the extremal inductance values recorded at room temperature reach -630 and 513 nH, which are comparable to those of commercial inductors. Figure 5(d) shows the film-width dependence of inductance change based on Figs. 5(a)–5(c) and S6. The EML effect is inversely proportional to the thin-film width. Given the film width is proportional to the thin-film area, this observation indicates the existence of an inverse size scaling law, a phenomenon consistent with prior findings reported in $Gd_3Ru_4Al_{12}$ (Ref. 2). Our theoretical calculations, founded on the concept of emergent inductance arising from transient domain wall motion, aptly elucidate the observed EML results.

In summary, we have observed the EML effect in Py/PC by manipulating transient domain walls through a stepwise magnetic field modulation. The inductance change reaches 1.1 μH and a noteworthy reversal in the sign of inductance within the vicinity of the zero magnetic field region. Moreover, we have demonstrated that the

dependence of the EML effect on frequency f, the step magnetic field jump ΔH, and film width w can be comprehensively explained through theoretical calculations based on the concept of the spin motive force arising from transient domain wall motion. Our study not only contributes to the understanding of intriguing fundamental physics but also holds promise for a wider range of the potential applications harnessing the EML effect.

See the supplementary material for a detailed exposition of the EML evaluation methodology, the magnetic response of reactance at $t_w = 1.0$ s, the frequency characteristics of EML curves, ΔH and w dependencies of EML curves at 12 and 24 kHz, respectively, and fitting parameters used in our calculations.

AUTHOR DECLARATIONS

Conflict of Interest

The authors have no conflicts to disclose.

Author Contributions

Yu Matsushima: Conceptualization (equal); Data curation (lead); Formal analysis (lead); Investigation (lead); Methodology (lead); Validation (lead); Visualization (lead); Writing – original draft (lead); Writing – review & editing (lead). **Zijing Zhang:** Data curation (equal); Formal analysis (equal); Investigation (equal); Methodology (lead); Validation (equal); Writing – review & editing (equal). **Yuri Ohashi:** Data curation (lead); Formal analysis (lead); Investigation (equal); Methodology (equal); Validation (equal); Writing – review & editing (equal). **Tsunagu Hatakeyama:** Data curation (lead); Formal analysis (lead); Investigation (equal); Methodology (lead); Validation (lead); Writing – review & editing (equal). **Gang Xiao:** Conceptualization (lead); Formal analysis (equal); Funding acquisition (lead); Methodology (equal); Project administration (equal); Supervision (equal); Validation (equal); Writing – original draft (equal); Writing – review & editing (lead). **Takumi Funato:** Conceptualization (equal); Data curation (equal); Formal analysis (lead); Funding acquisition (lead); Investigation (equal); Methodology (lead); Validation (lead); Writing – original draft (equal); Writing – review & editing (equal). **Mamoru Matsuo:** Conceptualization (equal); Formal analysis (lead); Funding acquisition (lead); Investigation (equal); Methodology (lead); Supervision (equal); Validation (equal); Writing – original draft (equal); Writing – review & editing (equal). **Hideo Kaiju:** Conceptualization (lead); Data curation (equal); Formal analysis (equal); Funding acquisition (lead); Investigation (equal); Methodology (lead); Project administration (lead); Supervision (lead); Validation (lead); Visualization (lead); Writing – original draft (lead); Writing – review & editing (lead).

DATA AVAILABILITY

Data that support the findings of this study are available from the corresponding author upon reasonable request.

REFERENCES

[1] N. Nagaosa, Jpn. J. Appl. Phys., Part 1 **58**, 120909 (2019).

[2] T. Yokouchi, F. Kagawa, M. Hirschberger, Y. Otani, N. Nagaosa, and Y. Tokura, Nature **586**, 232 (2020).

[3] J. Ieda and Y. Yamane, Phys. Rev. B **103**, L100402 (2021).

[4] D. Kurebayashi and N. Nagaosa, Commun. Phys. **4**, 260 (2021).

[5] A. Kitaoria, N. Kanazawa, T. Yokouchi, F. Kagawa, N. Nagaosa, and Y. Tokura, Proc. Natl. Acad. Sci. U. S. A. **118**, e2105422118 (2021).

[6] A. Kitaori, J. S. White, N. Kanazawa, V. Ukleev, D. Singh, Y. Furukawa, T. Arima, N. Nagaosa, and Y. Tokura, Phys. Rev. B **107**, 024406 (2023).

[7] A. Stern, Phys. Rev. Lett. **68**, 1022 (1992).

[8] S. E. Barnes and S. Maekawa, Phys. Rev. Lett. **98**, 246601 (2007).

[9] S. A. Yang, G. S. D. Beach, C. Knutson, D. Xiao, Q. Niu, M. Tsoi, and J. L. Erskine, Phys. Rev. Lett. **102**, 06720 (2009).

[10] Y. Yamane, J. Ieda, and A. Maekawa, Phys. Rev. B **88**, 014430 (2013).

[11] K. M. D. Hals and A. Brataas, Phys. Rev. B **91**, 214401 (2015).

[12] R. E. Gladyshevskii, O. R. Strusievicz, K. Cenzual, and E. Parthé, Acta Crystallogr. Sect. B **49**, 474 (1993).

[13] J. Niermann and W. Jeitschko, J. Inorg. Gen. Chem. **628**, 2549 (2002).

[14] S. Nakamura, N. Kabeya, M. Kobayashi, K. Araki, K. Katoh, and A. Ochiai, Phys. Rev. B **98**, 054410 (2018).

[15] V. Chandragiri, K. K. Iyer, and E. V. Sampathkumaran, J. Phys.: Condens. Matter **28**, 286002 (2016).

[16] M. Hirschberger, T. Nakajima, S. Gao, L. Peng, A. Kikkawa, T. Kurumaji, M. Kriener, Y. Yamasaki, H. Sagayama, H. Nakao, K. Ohishi, K. Kakurai, Y. Taguchi, X. Yu, T. Arima, and Y. Tokura, Nat. Commun. **10**, 5831 (2019).

[17] Y. Yamane, S. Fukami, and J. Ieda, Phys. Rev. Lett. **128**, 147201 (2022).

[18] M. Knobel and K. R. Pirota, J. Magn. Magn. Mater. **242–245**, 33 (2002).

[19] J.-Y. Chen, Y.-C. Lau, J. M. D. Coey, M. Li, and J. Wang, Sci. Rep. **7**, 42001 (2017).

[20] Y. Satake, K. Fujiwara, J. Shiogai, T. Seki, and A. Tsukazaki, Sci. Rep. **9**, 3282 (2019).

[21] S. Ota, A. Ando, T. Sekitani, T. Koyama, and D. Chiba, Appl. Phys. Lett. **115**, 202401 (2019).

[22] Y. Ohashi, Y. Matsushima, and H. Kaiju, J. Magn. Magn. Mater. **570**, 170497 (2023).

[23] X. Chen, B. Wang, X. Wen, P. Sheng, D. Pravarthana, H. Yang, Y. Xie, H. Liu, X. Xu, and R.-W. Li, J. Magn. Magn. Mater. **505**, 166750 (2020).

[24] H. Kaiju, A. Ono, N. Kawaguchi, K. Kondo, A. Ishibashi, J. Won, A. Hirata, M. Ishimaru, and Y. Hirotsu, Appl. Surf. Sci. **255**, 3706 (2009).

[25] H. Kaiju, N. Basheer, K. Kondo, and A. Ishibashi, IEEE Trans. Magn. **46**, 1356 (2010).

[26] L. Berger, Phys. Rev. B **33**, 1572 (1986).

[27] G. Tatara and H. Kohno, Phys. Rev. Lett. **92**, 086601 (2004).

[28] G. Tatara, T. Takayama, H. Kohno, J. Shibata, Y. Nakatani, and H. Fukuyama, J. Phys. Soc. Jpn. **75**, 064708 (2006).